IEEE Access
Multidisciplinary | Rapid Review | Open Access Journal

Received October 16, 2017, accepted November 26, 2017, date of publication December 6, 2017,
date of current version February 14, 2018.

Digital Object Identifier 10.1109/ACCESS.2017.2780286

A Nonlinear Decoupling Control Approach Using RBFNNI-Based Robust Pole Placement for a Permanent Magnet In-Wheel Motor

YONG LI[1], BIN LI[2], XING XU[1], AND XIAODONG SUN[1], (Member, IEEE)
[1]Automotive Engineering Research Institute, Jiangsu University, Zhenjiang 212013, China.
[2]Department of Mechanical Engineering, Concordia University, Montreal, QC H3G 1M8, Canada.

Corresponding author: Yong Li (liyongthinkpad@outlook.com)

This work was supported in part by the Natural Science Foundation of Jiangsu Province under Grant BK20160525, in part by the "333" Project of Jiangsu Province under Grant BRA2016445, in part by the Open Research Subject of Key Laboratory of Vehicle Measurement, Control and Safety of Sichuan Province under Grant SZJJ2017-076, in part by the Primary Research & Development Plan of Jiangsu Province under Grant BE2017129, and in part by the Initial Funding for Advanced Talents at Jiangsu University under Grant 15JDG164.

ABSTRACT This paper presents a novel nonlinear decoupling control scheme for a permanent magnet in-wheel motor (PMIWM), in which both the radial basis function neural network inverse (RBFNNI) and the state feedback robust pole placement (RPP) are employed. First, a theoretical analysis shows the existence of the inverse system of the PMIWM to be modeled mathematically. An inverse system is introduced into the original system of the PMIWM. Then, by cascading the RBFNNI system on the left side of the original PMIWM system, a new decoupling pseudo-linear system is established. Moreover, the RPP theory is employed to design an extra controller which further improves the disturbance rejection and robustness of the whole system. The effectiveness of the proposed control approach is verified by the real-time hardware-in-the-loop experiments under various operations.

INDEX TERMS Permanent magnet in-wheel motor, inverse system, radial basis function neural network, robust pole placement, electric vehicle.

I. INTRODUCTION

In recent years, electrified vehicles (EVs) have been regarded as one key technology in reducing future emissions and energy consumption in the mobility field. Generally, the drive system of EVs could be classified into centralized motor drive and in-wheel motor drive. The reduction and differential gear are coupled to the motor, which constitutes the centralized motor drive system. Compared with the centralized motor drive system, the in-wheel motor drive consists of the independent power electronics control system, which eliminates the mechanical transmission and drives the vehicle directly with faster torque response and higher efficiency. The in-wheel configuration has drawn significant attention from both industrial and academic researcher. Prominent features, such as high efficiency, high torque density and good overload capability, make the permanent magnet synchronous motor (PMSM) become a promising candidate for direct-drive propulsion [1], [2].

PMIWM, however, is a high-order, strongly coupled and nonlinear system. The accuracy of the controller is seriously influenced by the various uncertainties and nonlinearities of the PMIWM, which leads to great difficulties to achieve a strong robustness and disturbance rejection [3], [4]. To enhance the robustness of the control system, much effort has been made to address the above-mentioned drawbacks. Li *et al.* [5] and Chen *et al.* [6], [7] proposed some feedforward control methods to effectively deal with the disturbances and torque ripples. Several advanced feedback control techniques have been developed to improve the performance of the PMIWM in recent years, such as direct torque control, dynamic programming, model predictive control, sliding mode control, model reference adaptive control, fuzzy logic control, artificial neural network control [8], [9]. Ammar *et al.* [10] and Khedher and Mimouni [11] employed direct torque control (DTC) to achieve dynamic decoupling the induction motor. However, DTC has the shortcomings of a poor low-speed performance and large torque ripple [10], [11]. Incremental optimization methods and parametric structures are hybridized to approximate the system control [12], [13]. Model predictive control (MPC) can

explicitly handle constraints based on the future dynamic behavior of the system. However, MPC involves much computation load and long processing time, and could mainly be suitable for the linear system [15]–[17]. Sliding mode control (SMC) method is applied to the speed control of the brushless DC motor [15]–[17]. SMC improves the robustness of the speed control system, but its inherent high-frequency chattering is difficult to eliminate. Model reference adaptive control (MRAC) technique is mature and easy to be implemented [21], [22]. The adjustment of the adaptive parameters is related to the error and derivative of the error. The tracking performance of the speed control system is improved after introducing the adaptive law, which overcomes the deterministic dependence of the optimal control of the controlled object and the environment model and is more adaptable. But, MRAC depends on the fixed parameters and structure of the system. The system will fall into complex calculations when the system model is unknown.

Aiming to address the above-mentioned drawbacks, the intelligent control schemes have been developed in recent years. Fuzzy logic control (FLC) can get better speed tracking effect than other control schemes. The design of fuzzy logic control, however, lacks systematic methods [23]. The determination of the membership function and fuzzy rule mainly depend on the experts' experience. The impact of the nonlinear factors on the system performance could not be fundamentally weakened [24]. Neural network control (NNC) can improve the performance by parallel and distributed processing learning, which does not require mathematical models [25]–[29]. In [30] and [31], the back-propagation neural network (BPNN) is used for dynamic decoupling control of permanent magnet motor. Ben and Kurosawa [32] use BPNN-based speed estimator to control the speed of the motor. The BPNN is also employed in [30]–[32] to estimate the parameter for the dynamic system. BPNN, however, has the shortcomings of low learning rate, long convergence speed and easily trapping to a local minimum. The radial basis function neural network (RBFNN) is more suitable than multilayer neural networks due to its localized learning capability, which can work as the decoder [36]. The function approximation capability of the RBFNN has been proven and implemented to the dynamic nonlinear system in [37].

The linearization and decoupling control methods, including differential geometry scheme and inverse system scheme, have been widely used in magnetic bearings systems recently. The differential geometry is difficult to be implemented practically due to its abstract and complex process procedure. Moreover, the inverse system is relative to carry out in practice. However, the inverse system control approach requires an accurate mathematical model of the control plant, which could not be obtained precisely. Thus, the linearization and decoupling of the PMIWM are difficult to achieve by only utilizing the inverse system method. It is necessary to realize the dynamic decoupling control of the complex nonlinear system by investigating an effective and intelligent control scheme for the PMIWM control system. The combination of the inverse system and other intelligent method is supposed to realize the linearization and decoupling control of the PMIWM.

In this study, a novel radial basis function neural network inverse (RBFNNI) control scheme is adopted to implement the control system for the PMIWM. The RBFNNI control method combines the approximating ability of RBF neural network with the decoupling characteristic of the inverse system. The complex nonlinear system of the PMIWM will be decoupled into a pseudo-linear system using the proposed RBFNNI control scheme. In addition, as the unknown load dynamics and parameters variation affect the control performance of the PMIWM, the whole pseudo-linear system could not be completely decoupled. Since the performance of a feedback control system is largely determined by its closed-loop poles, robust pole placement is an effective state-space method for the feedback control design of the multivariable system. Thus, it is necessary to combine the RBFNNI control scheme with pole assignment method in the dynamic decoupling control of the PMIWM.

The paper is organized as follows. First, in Section 2, the PMIWM modeling and invertibility analysis are deduced. In Section 3, the RBFNNI control scheme is described. After that, the pole assignment method is presented in detail in Section 4. The HIL test bench is implemented, and the test results are presented and discussed in Section 5. Section 6 is devoted to the conclusions of the work.

II. INVERSE SYSTEM MODELING

A. MATHEMATICAL MODEL OF THE PMIWM

The following assumptions are made to simplify the mathematical model of the PMIWM: 1) The air gap magnetic field, produced by the permanent magnet and the armature reaction, distributes as a sine wave. The induced electromotive force generated by the winding flux of the three-phase stator is also supposed to distribute as a sine wave. 2) The stator magnetic circuit saturation and iron loss can be ignored due to its large air gap. 3) There is no damper winding on the rotor and no damping effect on the permanent magnet.

The mathematical model of the PMIWM in the synchronously rotating d-q reference frame is expressed as Eq. (1):

$$\begin{cases} u_d = R_s i_d - L i_q \omega + L\dot{i}_d \\ u_q = R_s i_q - L i_d \omega - \psi_f \omega + L\dot{i}_q \\ J_M \dot{\omega} = \dfrac{3}{2} p_n^2 \psi_f i_q - p_n T_L \end{cases} \tag{1}$$

where i_d and i_q are the d-axis and q-axis current of the stator, respectively. u_d and u_q represent voltage component on the d-axis and q-axis, respectively. ω denotes the electrical angular velocity of the PMIWM rotor. L indicates the inductance of the d-axis and q-axis, respectively. R_s shows the resistance of the stator. ϕ_f means the permanent magnet flux linkage of the rotor. J_M denotes the moment inertia of the PMIWM and T_L is the load torque. p_n is the number of pole pairs.

The PMIWM is controlled by the field oriented control (FOC) method shown in Fig. 1. Double closed-loop control of current and speed is employed for the PMIWM. The inner closed loop is an automatic current regulator (ACR) and the outer closed loop is automatic speed regulator (ASR). The two inputs of the ACR are the errors of the q-axis and d-axis current. The two outputs of the ACR are q-axis voltage and d-axis voltage command. The input of the ASR is the speed error e. The output of the ASR is a q-axis current command (motor torque command) i_q^*. The inputs of the whole system are speed reference ω^* and d-axis current command i_d^*. The outputs of the system are speed feedback ω and d-axis current feedback i_d.

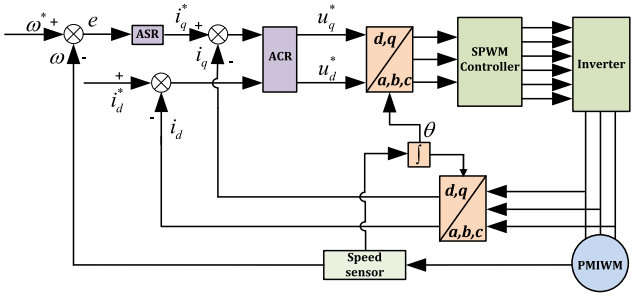

FIGURE 1. Block diagram of the PMIWM.

B. ANALYSIS OF THE PMIWM INVERTIBILITY

The dynamic model of the PMIWM, in view of the functional analysis, could be expressed by a mapping from the inputs to the outputs [30], [31]. Assume a linear or nonlinear system $\sum$ has a p-dimensional input vector $u = (u_1, u_2, \cdots u_q)$, a q-dimensional output vector $y = (y_1, y_2, \cdots y_q)$ and an initial state vector $x(t_0) = x_0$. Let $\theta : u \to y$; be the operator describing the aforementioned mapping relation.

$$y(\bullet) = \theta\,[x_0, u(\bullet)] \quad \text{or } y = \theta u \tag{2}$$

The inverse system is to realize the mapping from the output y to the input u.

Definition 1: Consider a system $\sum$ expressed by Eq. (2). Assume $\prod$ is another system with $y(t)$ as the input and $u(t)$ as the output. It could be expressed by an operator $\overline{\theta} : y \to u$, where $y_d = (y_{d1}, y_{d2}, \cdots y_{dq})$, $u_d = (u_{d1}, u_{d2}, \cdots u_{dq})$. y_d could be any vector composed of smooth functions. If the operator $\overline{\theta}$ satisfies

$$\theta\overline{\theta} y_d = \theta u_d = y_d \tag{3}$$

The system $\prod$ could be defined as an inverse system of the original system $\sum$, which means the original system $\sum$ is invertible.

Definition 2: Assume $\sum_\alpha$ is another mapping $u_d = \overline{\theta_\alpha}\varphi$ with q-dimensional input and p-dimensional output, where $\varphi = (\varphi_1, \varphi_2, \cdots \varphi_q)$, $u_d = (u_{d1}, u_{d2}, \cdots u_{dp})$. φ is any vector of a continuous function in a region and satisfies a certain initial condition at time t_0. If θ_α satisfies:

$$\theta\overline{\theta_\alpha}\varphi = \theta\overline{\theta_\alpha}(y_d^{(\alpha)}) = \theta u_d = y_d \tag{4}$$

Then $\prod_\alpha$ is the α-order inverse system of the system $\sum$. The α-order inverse system is easily implemented because the general nonlinearity is hybridized by a group of nonlinear mapping and a pure integral block.

The newly established composite system composes of an α-order inverse system $\prod_\alpha$, and, cascaded with its original system $\sum$, is called an α-order pseudo-linear system. Based on Eq. (4), the system $\sum \overline{\sum_\alpha}$ described by the mapping $\theta\overline{\theta_\alpha}$ is a linear system, which is equivalent to the system cascaded by the α integrator.

The inverse system control approach is a nonlinear control strategy, a direct feedback-linearization method. As a multi-input-multi-output (MIMO) system, the α-order inverse systems are generally realized by the state feedback. A pseudo-linear system in series is generated by putting α-order inverse system before the original system.

The inverse system method provides the possibility of feedback linearization and multivariable decoupling for the complex nonlinear systems. The pseudo-linear hybrid system can be obtained by putting the generalized inverse system on the left side of the original system. Then the linearization and decoupling of the nonlinear system can be realized. The dynamic decoupling control of the PMIWM can be implemented by using the inverse system approach, which is a direct feedback linearization approach. The accurate mathematical model of the controlled object is required for the realization of decoupling linearization. Therefore, the reversibility of the mathematical model of the PMIWM should be discussed firstly [3], [4], [30], [38].

The control purpose is to decouple the speed ω, the d axis current i_d, the q axis current i_q, and the flux ψ_f. Thus, i_d and ω are the outputs of the PMIWM, whose variables are $y = [y_1, y_2]^T = [i_d, \omega]^T$. Furthermore, u_d and u_q are selected as the control variables, where $u = [u_1, u_2]^T = [u_d, u_q]^T$, while i_d, i_q and ω are state variables, where $x = [x_1, x_2, x_3]^T = [i_d, i_q, \omega]^T$.

The differential of the output is written as

$$\begin{cases} \dot{y_1} = \dot{x_1} = \dfrac{u_1 - R_s x_1 + L x_2 x_3}{L} \\ \dot{y_2} = \dot{x_3} = \dfrac{3p_n^2\psi_f x_2 - 2p_n T_L}{2J_M} \\ \ddot{y_2} = \ddot{x_3} = \dfrac{3}{2}\dfrac{p_n^2\psi_f}{J_M}\dfrac{\left(u_2 - R_s x_2 + \psi_f x_3 - L x_1 x_3\right)}{L} \end{cases} \tag{5}$$

According to the theory of the inverse system, the determ of the Jacob matrix $A(x, u)$ of Eq. (5) could be expressed as

$$Det\,[A(x,u)] = \frac{3}{2J_M L^2} p_n^2 \psi_f \tag{6}$$

The flux ψ_f of the PMWIM could not be zero, such that $A(x, u)$ is a nonsingular matrix. The relative order of the system is $\alpha = (\alpha_1, \alpha_2) = (1, 2)$. As a result of $\sum_{i=1}^{2} \alpha_i = 3 \le n$,

n is the number of the state variable, which satisfies the sufficient conditions of the existence of the inverse system.

III. RBFNNI-BASED DECOUPLING SCHEME OF PMIWM

The PMIWM, however, still cannot be completely decoupled even if its inverse system has been expressed in the above section. Furthermore, the parameter perturbations, load disturbance and unmodeled dynamics may influence the performance of the motor. Therefore, the RBFNNI, in this section, is introduced to address these problems.

A. RADIAL BASIS FUNCTION NEURAL NETWORK (RBFNN)

Recently, RBFNN has attracted more consideration due to its simple structure and perfect generalization ability, which has been utilized in practical applications. RBFNN can approximate any nonlinear function with arbitrary accuracy. The stability of the system and the convergence of the weight coefficient can be guaranteed by the adaptation law [37].

RBF neural network shown in Fig. 2 has three layers: the input layer, the hidden layer and the output layer. The hidden layer consists of several hidden nodes, which contain a center c vector that is a parameter vector of the same dimension as the input vector x is defined by $\|x(t) - c_j(t)\|$.

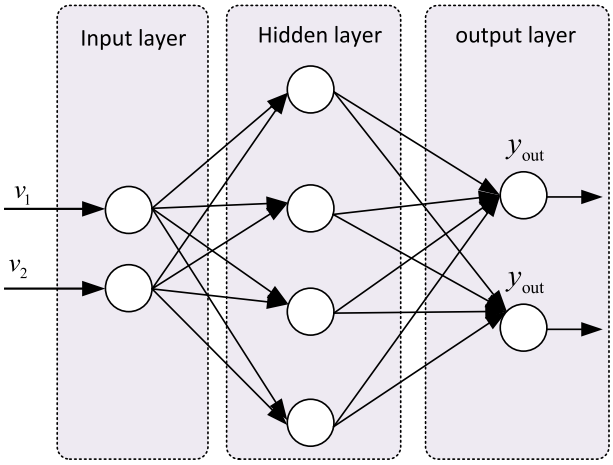

FIGURE 2. The topological structure of the RBFNN.

The output of the hidden layer can be obtained by a nonlinear activation function $h_j(t)$ expressed as follows:

$$h_j(t) = \exp\left(-\frac{\|x(t) - c_j(t)\|^2}{2b_j^2}\right), \quad j = 1, \ldots, m \tag{7}$$

Where $\|\bullet\|$ is the Euclidean norm. $x(t)$ is the i-th input. $c_j(t)$ is the middle of the k-th node in the hidden layer. b_j is a positive scalar. m is the hidden nodes number.

As a linear weighted combination, the output layer is expressed as:

$$y_i(t) = \sum_{j=1}^{m} w_i h_j(t) + \varepsilon = \sum_{j=1}^{m} w_i \exp\left(-\frac{\|x(t) - c_j(t)\|^2}{2b_j^2}\right) + \varepsilon, \quad i = 1, \ldots, n \tag{8}$$

where w is the output layer weight. n is the number of outputs. y is the network output. m is the total number of the nodes in the hidden layer. ε is the error between the ideal RBFNN, which is approximated by a real RBFNN $y_i^{\wedge}(t)$ with weight update laws to learn the ideal parameters, $\varepsilon \leq \varepsilon_N$.

RBFNN is adopted to the control system of the PMIWM. It is a fully connected feedback network where the output layer neurons have linear characteristics, but the hidden layer neurons use a radial basis function as the activation function. Usually, the RBFNN produces local mapping in contrast with the global mapping of a BP neural network. One advantage of the RBFNN is that its training is much faster and easier than the BP neural network.

B. RBFNN-BASED ADAPTIVE CONTROL

The RBFNN is established by using structure learning and parameter learning. The similarity between the newly generated membership function and the existing ones must be checked in the process of the structure learning. The parameter learning is used to adjust the connected weights in the consequent part, and the feedback weights and the parameters of the membership functions are employed to minimize a given energy function by the RBF algorithm [39]–[42].

The diagram of the RBFNN-based adaptive control scheme is shown in Fig. 3.

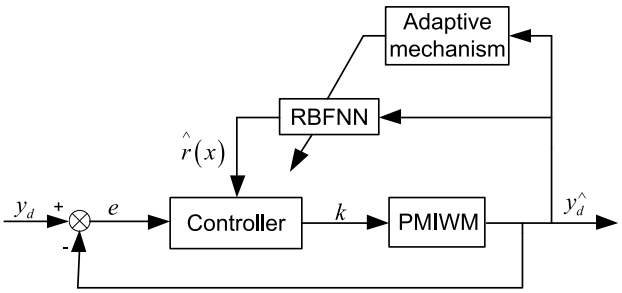

FIGURE 3. The diagram of the RBFNN-based adaptive control scheme.

Suppose the output of the RBFNN is described as

$$\hat{r}(x) = \hat{w}^T m(x) \tag{9}$$

Where $\hat{w}$ is the estimated parameter of w. $m(x)$ is the Gaussian function.

The stability of the RBFNN should be analyzed.

Let

$$Z = \begin{bmatrix} 0 & 1 \\ -i_p & -i_d \end{bmatrix}, \quad M = \begin{bmatrix} 0 \\ 1 \end{bmatrix} \tag{10}$$

The estimation error can be defined as

$$\omega = \hat{r}(x) - r(x) \tag{11}$$

The Lyapunov function can be designed as

$$V = \frac{1}{2}E^T Q E + \frac{1}{2\delta}(\hat{w} - w^*)^T(\hat{w} - w^*) \tag{12}$$

Where E is the error function, $E = (e, \dot{e})^T$. δ is a positive constant. w^* is the optimal weight. Q is a symmetric matrix, which satisfies the Lyapunov equation: $Z^T Q + QZ = -P$ and $P \geq 0$.

Then, the derivative V can be expressed as

$$\dot{V} = -\frac{1}{2} E^T P E + E^T Q M \omega \tag{13}$$

Since $-\frac{1}{2} E^T P E \leq 0$, $\dot{V} \leq 0$ will be obtained if the error ω is designed to be less than 10^{-4}.

C. RBFNNI SYSTEM

To take the advantages of the RBFNN control method and the inverse control approach, two schemes are combined to establish a novel decoupling control system. The RBFNN is employed to realize the reversibility of the PMIWM control system. By cascading some certain integrators before the RBFNN block, the novel NNI control system is established with the ability of generalization and will improve the robustness and fault-tolerant performance. The proposed NNI is located on the left side of the PMIWM shown in Fig. 4, which leads to a pseudo-linear system for the system decoupling. The NNI control approach can improve the robustness and reject the disturbance.

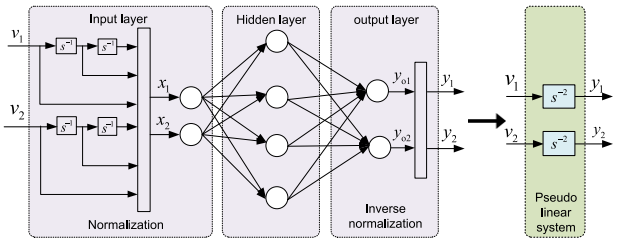

FIGURE 4. The pseudo-linear system.

The RBFNN is chosen as 2-4-2. The parameters of the RBFNN, including the learning rate and momentum coefficient can be optimized by trail-and-error. Three sets of data, selected from the selected drive cycle, are shown in Table 1 in the repaid changing area. The data are employed as the training sample of RBFNN. The input samples go into the network work periodically during the whole training process. The output error does not enter into the permitted range until the convergence of the neural network. The learning rate is set at 0.06 during the training process. The RBFNN is supposed to meet the requirement when the training error is less than 0.02 after 1000 epochs training. Therefore, the RBFNN is established successfully.

IV. ROBUST POLE PLACEMENT FOR PMIWM CONTROL

A. PRELIMINARIES

Pole placement is an effective state-space method for feedback control system design. The robust pole placement (RPP) problem for a linear system is to find the feedback gains. The state-feedback RPP problem is to find a state feedback matrix

TABLE 1. The training samples of RBFNN.

Number	Team 1	Team 2	Team 3
1	503.33	536.88	442.93
2	536.88	536.88	402.66
3	570.44	536.88	362.39
4	603.99	483.19	322.13
5	637.55	429.50	281.86
6	671.10	375.82	241.59
7	704.66	322.13	201.33
8	738.21	268.44	161.06
9	771.77	214.75	120.79

such that the eigenvalues of the linear closed-loop system matrix, associated with the closed-loop system are the given poles that closed under complex conjugate [43], [44].

Considering a control system expressed as Eq. (14) as follows:

$$\dot{x}(t) = Ax(t) + Bu(t), \quad x(0) = x_0 \tag{14}$$

where $x(t)(n \times 1)$ is the state vector, $u(t)$ is the scalar control variable, $A(n \times n)$ and $B(n \times 1)$ are system matrix and control gain vector, respectively. The characteristic polynomial of matrix A to the state feedback RPP is given by

$$\det[sI - A] = s^n + a_{n-1}s^{n-1} + \bullet\bullet\bullet + a_1 s + a_0 = 0 \tag{15}$$

Where $a = [a_0, a_1, \bullet\bullet\bullet, a_{n-1}]$ are the coefficients of the characteristic polynomial and I is the $(n \times n)$ identity matrix. The objective is to place the desired poles for the closed-loop system. The desired characteristic behavior for the states can be enforced by the constant state-feedback control.

The closed-loop characteristic polynomial solution to the SFRPP can be obtained by Eq. (16)

$$\det\left[sI - (I + BK)^{-1} A\right] = 0 \tag{16}$$

After the solution of the state feedback RPP, the departure is employed to measure the robustness from the normality of $\dot{x}(t)$, which can be expressed as Eq. (17)

$$\Delta u\left[\dot{x}(t)\right] = \sqrt{\left\|\dot{x}(t)\right\|_u^2 - \sum_{i=1}^{m} |\sigma_i|^2} \tag{17}$$

Where σ_i, $i = 1, \ldots, m$, are the poles to be placed.

B. RPP FOR LINEAR SYSTEM

The speed and flux can be approximated as a two input and two output linear system with minimum phase [45]. The input $U(k) = [i_{di}(k), \omega_i(k)]^T$, and the output $Y(k) = [i_{do}(k), \omega_o(k)]^T$.

The decoupling controller is designed as shown in Fig. 5. The output feedback matrix $H(z^{-1})$ and the pre-decoupling compensation matrix $L(z^{-1})$ could be realized, which makes sure the closed-loop transfer function $T(z^{-1})$ is a diagonal matrix. The single-loop controller (SLC) $C(z^{-1})$ is designed

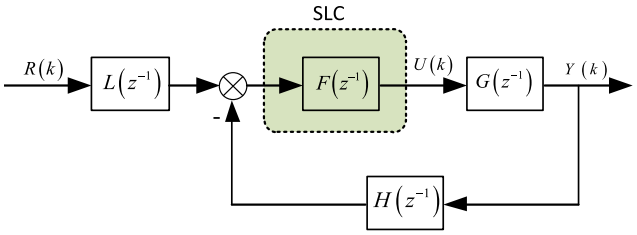

FIGURE 5. The diagram of decoupling control system.

TABLE 2. The parameters of the PMIWM.

Parameter	Value	Unit	Description
P_N	8	kW	Nominal Power
P_n	2	pair	Pole pair number
f_n	50	Hz	Nominal frequency
V_n	72	V	Nominal Voltage
n_n	1600	rpm	Nominal Speed
T_n	100	Nm	Nominal Torque
J_M	0. 08	kg·m^2	Moment of Inertia

according to the dynamic and static performance requirements of each channel.

The closed-loop transfer function of the decoupling is written as

$$O(z^{-1}) = \left[M(z^{-1}) + N(z^{-1})H(z^{-1})\right]^{-1} N(z^{-1})L(z^{-1}) \tag{18}$$

Where $M(z^{-1})$ and $N(z^{-1})$ are the matrix polynomial determined by the system parameters.

Assuming the supposed closed-loop transfer function after pole placement is described as

$$O_e(z^{-1}) = M_e^{-1}(z^{-1})N_e^{-1}(z^{-1}) \tag{19}$$

Where, M_e^{-1} and N_e^{-1} are diagonal constant matrix, respectively.

To ensure $O(z^{-1}) = O_e(z^{-1})$, the M_e^{-1} and N_e^{-1} are written as

$$\begin{cases} M_e(z^{-1}) = M(z^{-1}) + M(z^{-1})H(z^{-1}) \\ N_e(z^{-1}) = N(z^{-1})L(z^{-1}) \end{cases} \tag{20}$$

Polynomial division calculation, however, will be involved in the solution of $L(z^{-1})$ and $H(z^{-1})$, which could be obtained by Eq. (20). A stable filter $\frac{1}{f(z^{-1})}$ is employed into each channel of $F(z^{-1})$ to ease the finite order solution process. $f\left(z^{-1}\right) = f_0 + f_1 z^{-1} + f_2 z^2 + \cdots$ and $f_0 \neq 0$.

If $f(z^{-1}) = n_0 + n_1 z^{-1} + n_2 z^{-2} + \cdots$, the finite order solutions of $L(z^{-1})$ and $H(z^{-1})$ are expressed as

$$\begin{cases} H(z^{-1}) = z^d(\text{adj}N(z^{-1}))\left[M_e(z^{-1}) - M(z^{-1})\right] \\ L(z^{-1}) = z^d(\text{adj}N(z^{-1}))N_e(z^{-1}) \end{cases} \tag{21}$$

The two-input and two-output linear system could be decoupled into two independent subsystems by the above-mentioned $L(z^{-1})$, $H(z^{-1})$ and $f(z^{-1})$.

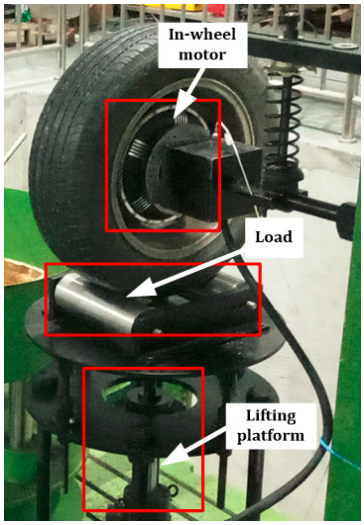

FIGURE 6. The dSPACE-based HIL test bench.

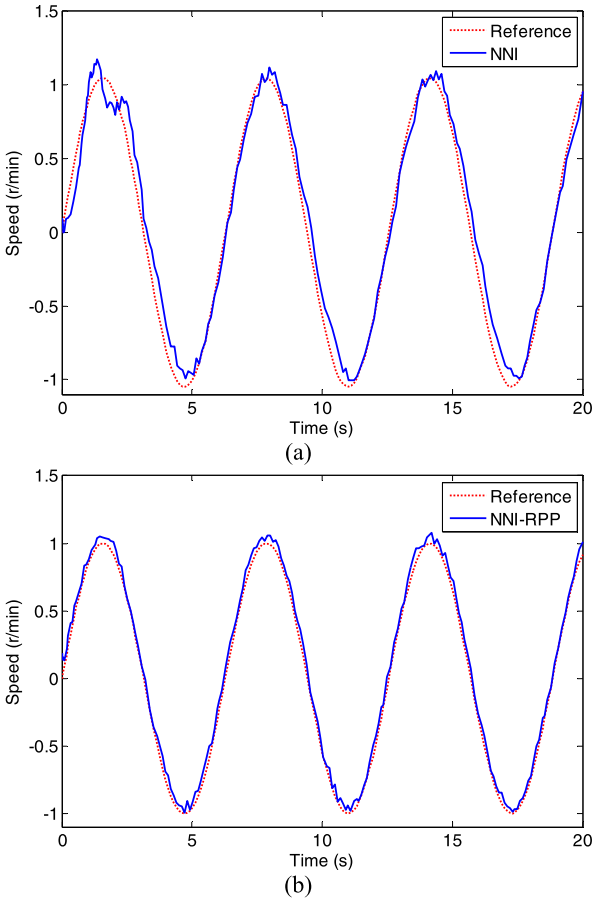

FIGURE 7. Speed tracking performance with sine wave reference. (a) NNI control. (b) Proposed control scheme.

V. EXPERIMENTAL VALIDATION

To validate the effectiveness and the performance of the proposed RBFNNI-based robust pole placement control scheme of the PMIWM, hardware-in-the-loop (HIL) tests are carried out below.

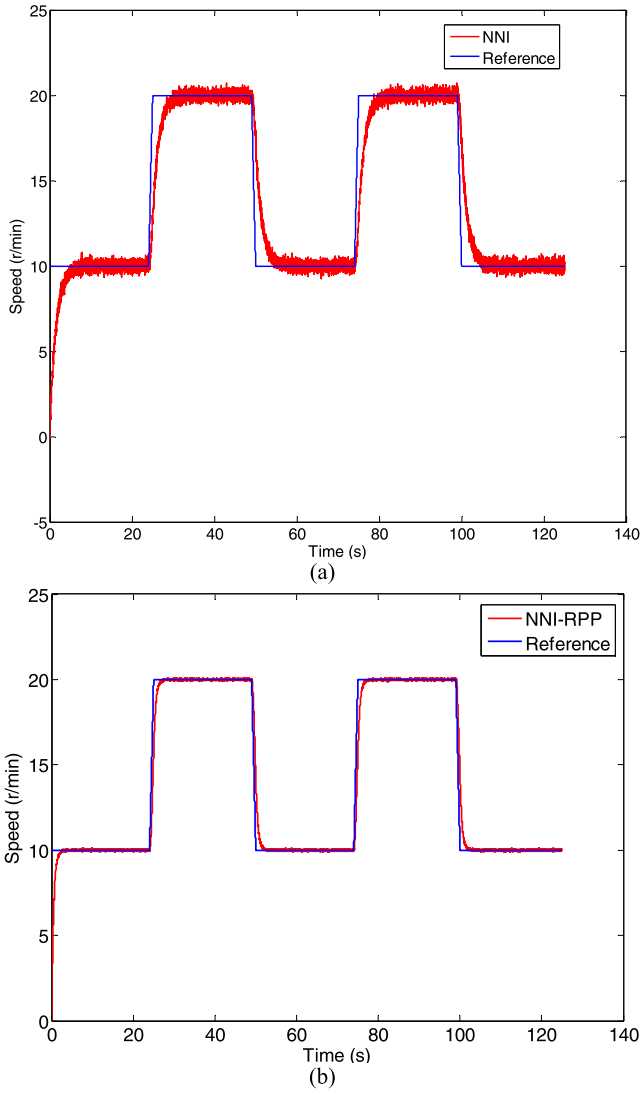

FIGURE 8. Speed tracking performance with square wave reference. (a) NNI control. (b) Proposed control scheme.

A. EXPERIMENTAL SETUP

A dSPACE-based HIL test bench is built, which consists of a user PC, a dSPACE hardware, a control box, and a control console. The dSPACE real-time test bench is used as the control module, the PWM waves used to control the PMIWM are generated by the control strategies implemented to the motor control system. The Encoder board is used to convert the speed signal of the PMIWM installed inside the wheel hub. The parameters of the PMIWM is illustrated in Table.2. The dSPACE-based HIL test bench is shown in Fig. 6.

B. EXPERIMENT 1: TRACKING PERFORMANCE

To test the tracking performance of the PMIWM control system, comparative experiments with different speed reference and control schemes were carried out on the test bench respectively. The sine ware, square wave and constant value are selected as the reference speed.

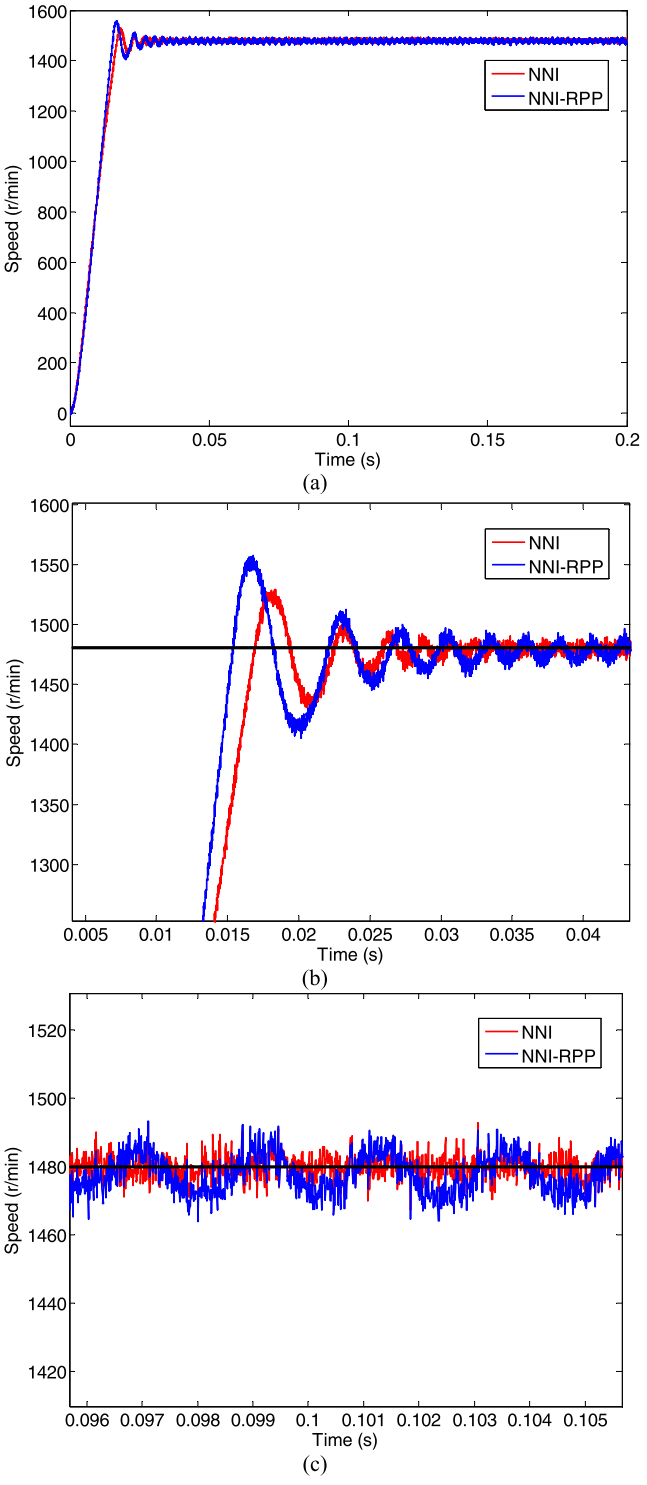

FIGURE 9. Speed tracking performance with constant speed reference. (a) Measurement speed. (b) Close-up at 0.02s. (c) Steady-state close-up at 0.1s.

Fig. 7 shows the speed trajectory with sine wave reference. Fig. 7(a) demonstrates that the feedback speed cannot completely follow the reference under RBFNNI control scheme, especially at the startup experiment from 0s to 2.2s. Compared with Fig. 7(a), the feedback speed under the proposed

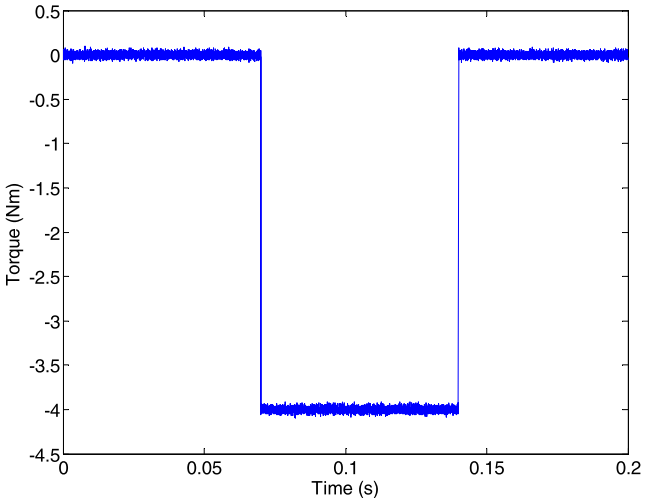

FIGURE 10. Measurement torque.

RBFNNI-RPP control scheme follows the reference very well except for the beginning testing from 0s to 2.2s. Comparison results obviously illustrate that although there are some large fluctuations in the feedback speed under the proposed control scheme shown in Fig. 7(b) from 0s to 2.2s, which is caused by the moment of inertia of the PMIWM. Fig. 7 shows the control precision is effectively improved with the proposed control scheme.

The responses with square wave reference are shown in Fig. 8, which demonstrates that the actual speed under the RBFNNI and the proposed control scheme, respectively. Fig. 7(a) shows the measurement speed cannot completely agree with its reference at the rapidly changing spots during the operation. The response time is approximately 4.8s in Fig. 8(a) and 1.6s in Fig. 8(b), which demonstrates the proposed control scheme can compute the solutions rapidly and greatly shorten the delay. In addition, there is also high noise level in the feedback speed. Compared with the RBFNNI control scheme, From Fig. 8, it is obviously found that in Fig. 8 the tracking error with proposed control scheme is reduced by 90%, as well as the noise level is decreased by 80% which illustrates the steady-state peak displacement of the PMIWM.

In this experiment, constant speed is also employed as the reference for analyzing the speed tracking ability of the proposed control scheme. Fig. 9 shows the measurement speed with the RBFNNI control approach has a smaller overshoot and fluctuation than the proposed control method. However, the RBFNNI control scheme performs well in terms of the response time than the proposed control method.

C. EXPERIMENT 2: DISTURBANCE REJECTING ABILITY

In this section, experiments are carried out to verify the performance of disturbance rejecting ability with a sudden load impact on the control system. To verify the load disturbance rejection, the PMIWM is started without any load, and 4Nm is applied suddenly at 0.07s which lasts for 0.07s.

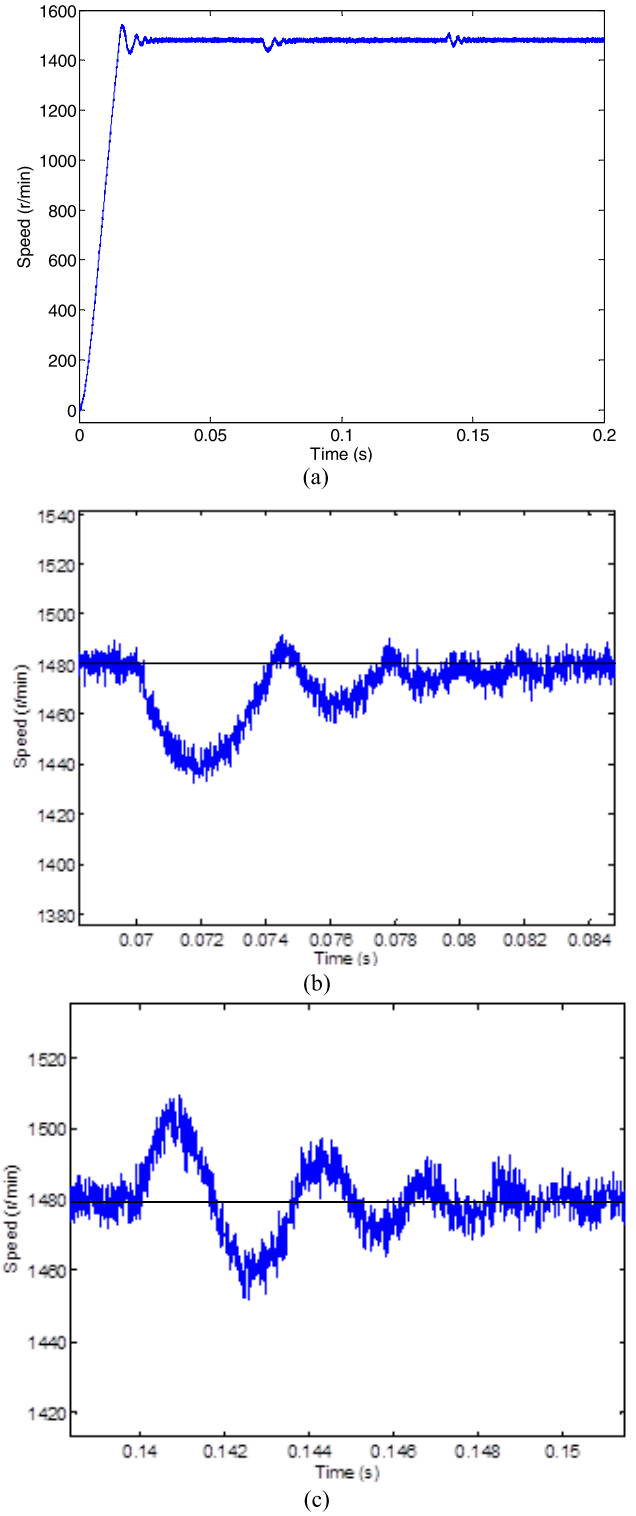

FIGURE 11. Disturbance rejecting ability (a) Measurement speed with the NNI control scheme. (b) Close-up at 0.07s. (c) Close-up at 0.14s.

After that, the torque implemented on the motor is removed. Fig. 10 shows the curve of the load disturbance employed in the experiment. The experiment results of disturbance rejecting ability with the RBFNNI and the proposed control scheme are shown in Fig. 11 and Fig. 12.

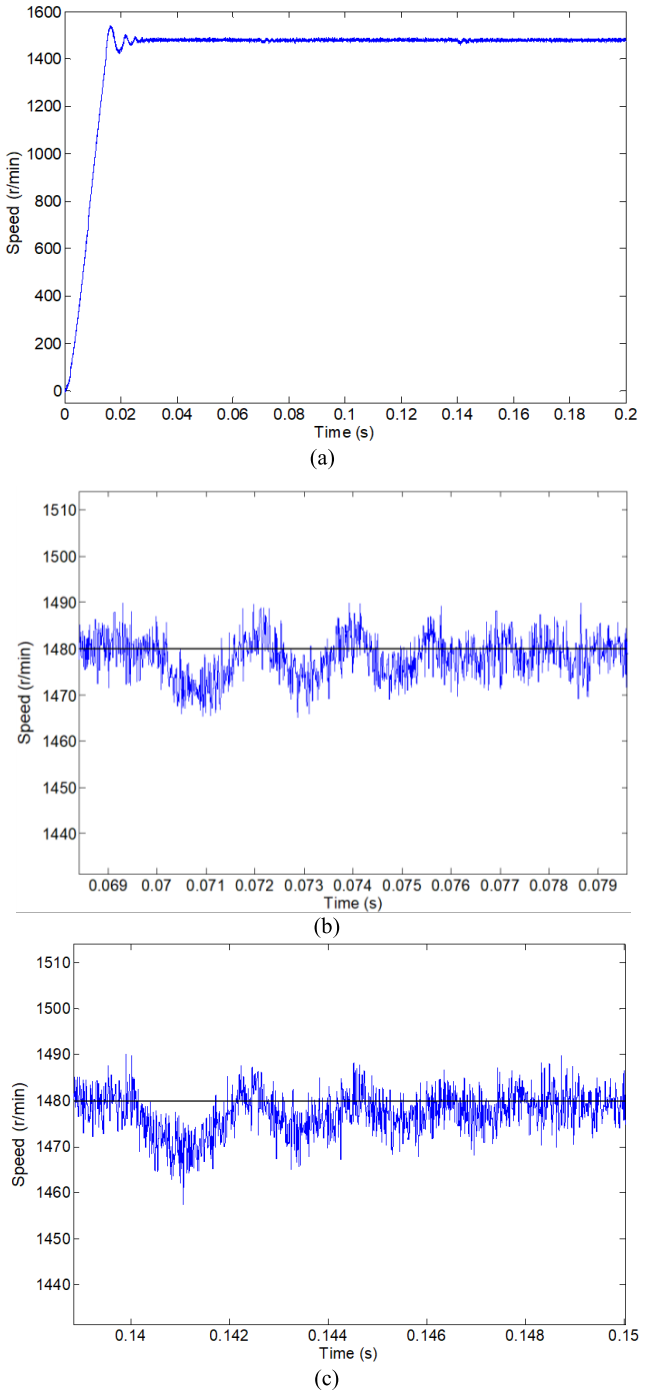

FIGURE 12. Disturbance rejecting ability (a) Measurement speed with the proposed control scheme. (b) Close-up at 0.07s. (c) Close-up at 0.14s.

It can be obviously seen from Fig. 11(a) that the output speed cannot completely avoid the sudden torque impact to the control system with the RFBNNI control approach. The amplified speed trajectory at t = 0.07s and t = 0.14s are shown in Fig. 11(b) and Fig. 11(c). The speed response experiences a large overshoot of 3.04% at 0.07s and 2.07% at 0.14s, respectively. The settling time as shown in Fig. 11(b) and Fig. 11(c) is 0.013s and 0.008s, respectively.

Fig. 12(a) shows that the speed fluctuations under the proposed control are much smaller than those in Fig. 11(a) at t = 0.07s and t = 0.14s when the loads are applied. As is seen in Fig. 12(b) and Fig. 12(c), the close-ups illustrate that the speed response has a large overshoot of 1.02% at 0.07s and 1.09% at 0.14s, respectively. It could be noted that in Fig. 12(b) and Fig. 12(c) the settling time is 0.009s and 0.008s, respectively.

Compared with the RBFNNI control approach, it can be obviously seen that the proposed RBFNNI-based RPP control scheme has prominent advantages in trajectory tracking and disturbance rejecting ability.

VI. CONCLUSION

To improve the control properties of high-accuracy, fast response and strong robustness for the PMIWM, a novel dynamic decoupling approach is developed based on the RBFNNI method for the synthesis of the pseudo-linear system via RPP in this paper. The experimental results obviously demonstrate the following: Firstly, the proposed control scheme can successfully realize the decoupling control of the PMIWM, which can avoid the shortcomings of the single RBFNNI control scheme. Secondly, by introducing the RPP method for the pseudo-linear system, the decoupling precision can be effectively improved, as well as the superiority of the elimination of the unmodeled dynamics. Thirdly, the proposed control scheme can theoretically and experimentally guarantee to find the global minimum regardless of the initial conditions, and provides a fast and computationally efficient solution. Moreover, inspired by the concept of the machine learning, further investigations will be focused on the RBFNN control, like layer number and neurons in each layer remain to be discussed in the future.

REFERENCES

[1] M. Ehsani, Y. Gao, and A. Emadi, *Modern Electric, Hybrid Electric, and Fuel Cell Vehicles-Fundamentals, Theory and Design*, 2nd ed. Boca Raton, FL, USA: CRC Press, 2010.

[2] B. Li, A. Goodarzi, A. Khajepour, S.-K. Chen, and B. Litkouhi, "An optimal torque distribution control strategy for four-independent wheel drive electric vehicles," *Veh. Syst. Dyn.*, vol. 53, no. 8, pp. 1172–1189, Apr. 2015.

[3] X. Sun, L. Chen, H. Jiang, and Z. Yang, "High-performance control for a bearingless permanent magnet synchronous motor using neural network inverse scheme plus internal model controllers," *IEEE Trans. Ind. Electron.*, vol. 63, no. 6, pp. 3479–3488, Jun. 2016.

[4] X. Sun, B. Su, L. Chen, Z. Yang, X. Xu, and Z. Shi, "Precise control of a four degree-of-freedom permanent magnet biased active magnetic bearing system in a magnetically suspended direct-driven spindle using neural network inverse scheme," *Mech. Syst. Signal Process.*, vol. 88, pp. 36–48, May 2017.

[5] X. Li, S.-L. Chen, C. S. Teo, and K. K. Tan, "Data-based tuning of reduced-order inverse model in both disturbance observer and feedforward with application to tray indexing," *IEEE Trans. Ind. Electron.*, vol. 64, no. 7, pp. 5492–5501, Jul. 2017.

[6] S.-L. Chen *et al.*, "Toward comprehensive modeling and large-angle tracking control of a limited-angle torque actuator with cylindrical Halbach," *IEEE/ASME Trans. Mechatronics*, vol. 21, no. 1, pp. 431–442, Feb. 2016.

[7] S.-L. Chen, K. K. Tan, S. Huang, and C. S. Teo, "Modeling and compensation of ripples and friction in permanent-magnet linear motor using a hysteretic relay," *IEEE/ASME Trans. Mechatronics*, vol. 15, no. 4, pp. 586–594, Aug. 2010.

[8] L. Wang, "Automatic tuning of PID controllers using frequency sampling filters," *IET Control Theory Appl.*, vol. 15, no. 5, pp. 835–842, 2017.
[9] Y. Li, F. Ma, and M. Khazerani, "Research on the control strategy for the traction motor on the test bench of vehicular energy storage system," *Proc. Chin. Soc. Electr. Eng.*, vol. 34, no. 21, pp. 3481–3487, Jul. 2014.
[10] A. Ammar, A. Bourek, and A. Benakcha, "Nonlinear SVM-DTC for induction motor drive using input-output feedback linearization and high order sliding mode control," *ISA Trans.*, vol. 67, pp. 428–442, Mar. 2017.
[11] A. Khedher and M. Mimouni, "Sensorless-adaptive DTC of double star induction motor original," *Energy Convers. Manage.*, vol. 51, no. 12, pp. 2878–2892, 2010.
[12] G. A. Revithank and M. A. Christodoulou, "Adaptive control of unknown plants using dynamical neural networks," *IEEE Trans. Syst., Man, Cybern.*, vol. 24, no. 3, pp. 400–411, Mar. 1994.
[13] H. D. Pariño and D. Liu, "Neural network-based model reference adaptive control system," *IEEE Trans. Syst., Man, Cybern. B, Cybern.*, vol. 30, no. 1, pp. 198–204, Feb. 2000.
[14] Y.-K. Choi, M.-J. Lere, S. Kim, and Y.-C. Kay, "Design and implementation of an adaptive neural-network compensator for control systems," *IEEE Trans. Ind. Electron.*, vol. 48, no. 2, pp. 416–423, Apr. 2001.
[15] C. A. Rojas, J. R. Rodriguez, S. Kouro, and F. Villarroel, "Multiobjective fuzzy-decision-making predictive torque control for an induction motor drive," *IEEE Trans. Power Electron.*, vol. 32, no. 8, pp. 6245–6260, Aug. 2017.
[16] Y. Huang, S. M. Fard, M. Khazraee, H. Wang, and A. Khajepour, "An adaptive model predictive controller for a novel battery-powered anti-idling system of service vehicles," *Energy*, vol. 127, pp. 318–327, May 2017.
[17] Y. Huang, A. Khajepour, F. Bagheri, and M. Bahrami, "Optimal energy-efficient predictive controllers in automotive air-conditioning/refrigeration systems," *Appl. Energy*, vol. 184, pp. 605–618, Dec. 2016.
[18] C.-L. Li and L. Wu, "Sliding mode control for synchronization of fractional permanent magnet synchronous motors with finite time," *Opt.-Int. J. Light Electron Opt.*, vol. 127, no. 6, pp. 3329–3332, 2016.
[19] K. M. A. Prasad, A. Unnikrishnan, and U. Nair, "Fuzzy sliding mode control of a switched reluctance motor," *Proc. Technol.*, vol. 25, pp. 735–742, Apr. 2016.
[20] Y. Huang, A. Khajepour, H. Ding, F. Bagheri, and M. Bahrami, "An energy-saving set-point optimizer with a sliding mode controller for automotive air-conditioning/refrigeration systems," *Appl. Energy*, vol. 188, pp. 576–585, Feb. 2017.
[21] R. Khanna, Q. Zhang, W. E. Stanchina, G. F. Reed, and Z.-H. Mao, "Maximum power point tracking using model reference adaptive control," *IEEE Trans. Power Electron.*, vol. 29, no. 3, pp. 1490–1499, Mar. 2014.
[22] C. Aguila and M. Duarte, "Improving the control energy in model reference adaptive controllers using fractional adaptive laws," *IEEE/CAA J. Autom. Sinica*, vol. 3, no. 3, pp. 332–337, Jul. 2016.
[23] B. Bose, *Modern Power Electronics and AC Drives*. Beijing, China: China Machine Press, 2006.
[24] A. Fadaei and K. Salahshoor, "A novel real-time fuzzy adaptive autotuning scheme for cascade PID controllers," *Int. J. Control Autom. Syst.*, vol. 9, no. 5, pp. 823–830, Oct. 2011.
[25] R. Sun, R. Song, and K.-Y. Tong, "Complexity analysis of EMG signals for patients after stroke during robot-aided rehabilitation training using fuzzy approximate entropy," *IEEE Trans. Neural Syst. Rehabil. Eng.*, vol. 22, no. 5, pp. 1013–1019, Sep. 2014.
[26] K.-H. Tan, "Squirrel-cage induction generator system using wavelet Petri fuzzy neural network control for wind power applications," *IEEE Trans. Power Electron.*, vol. 31, no. 7, pp. 5242–5254, Jul. 2016.
[27] E. Hartman, J. Keeler, and J. Kowalski, "Layered neural networks with Gaussian hidden units as universal approximations," *Neural Comput.*, vol. 2, no. 2, pp. 210–215, 1990.
[28] N. Hovakimyan, A. J. Calise, N. Kim, "Adaptive output feedback control of a class of multi-input multi-output systems using neural networks," *Int. J. Control*, vol. 77, no. 15, pp. 1318–1329, 2007.
[29] X. Fu and S. Li, "A novel neural network vector control technique for induction motor drive," *IEEE Trans. Energy Convers.*, vol. 30, no. 4, pp. 1428–1437, Dec. 2015.
[30] X. Sun, Z. Shi, L. Chen, and Z. Yang, "Internal model control for a bearingless permanent magnet synchronous motor based on inverse system method," *IEEE Trans. Energy Convers.*, vol. 31, no. 4, pp. 1539–1548, Dec. 2016.
[31] X. Sun, L. Chen, Z. Yang, and H. Zhu, "Speed-sensorless vector control of a bearingless induction motor with artificial neural network inverse speed observer," *IEEE/ASME Trans. Mechatronics*, vol. 18, no. 4, pp. 1357–1366, Aug. 2013.
[32] L. Ben and R. Kurosawa, "Identification of induction motor speed using neural networks," in *Proc. Power Convers. Conf.*, 1993, pp. 689–694.
[33] N. A. Abbasi, T. Landolsi, and R. Dhaouadi, "A neural network based technique for vibration characterization using Gaussian laser beams," *Mechatronics*, vol. 25, pp. 44–54, Feb. 2015.
[34] G. Pathak, B. Singh, and B. K. Panigrahi, "Back-propagation algorithm-based controller for autonomous wind-DG microgrid," *IEEE Trans. Ind. Appl.*, vol. 52, no. 5, pp. 4408–4415, Sep. 2016.
[35] B. Singh and S. R. Arya, "Back-propagation control algorithm for power quality improvement using DSTATCOM," *IEEE Trans. Ind. Electron.*, vol. 61, no. 3, pp. 1204–1212, Mar. 2014.
[36] S. Seshagiri and H. K. Khalil, "Output feedback control of nonlinear systems using RBF neural networks," *IEEE Trans. Neural Netw.*, vol. 11, no. 1, pp. 69–79, Jan. 2000.
[37] J. Park and I. W. Sandberg, "Universal approximation using radial-basis-function networks," *Neural Comput.*, vol. 3, no. 2, pp. 246–257, Mar. 1991.
[38] G. Liu, L. Chen, W. Zhao, Y. Jiang, and L. Qu, "Internal model control of permanent magnet synchronous motor using support vector machine generalized inverse," *IEEE Trans. Ind. Informat.*, vol. 9, no. 2, pp. 890–898, May 2013.
[39] J. Liu, *Radial Basis Function (RBF) Neural Network Control for Mechanical Systems*. Beijing, China: Tsinghua Univ. Press, 2013.
[40] A. Huang and Y. Chen, "Adaptive sliding control for single-link flexible joint robot with mismatched uncertainties," *IEEE Trans. Control Syst. Technol.*, vol. 12, no. 5, pp. 770–775, Sep. 2004.
[41] J. Liu and Y. Lu, "Adaptive RBF neural network control of robot with actuator nonlinearities," *J. Control Theory Appl.*, vol. 8, no. 2, pp. 249–256, 2010.
[42] Y. Wang, W. Sun, Y. Xiang, and S. Miao, "Neural network-based robust tracking control for robots," *Int. J. Intell. Autom. Soft Comput.*, vol. 15, no. 2, pp. 211–222, 2009.
[43] X. Le and J. Wang, "Robust pole assignment for synthesizing feedback control systems using recurrent neural networks," *IEEE Trans. Neural Netw. Learn. Syst.*, vol. 25, no. 2, pp. 383–393, Feb. 2014.
[44] Z.-C. Guo, J. Qian, Y.-F. Cai, and S.-F. Xu, "Refined Schur method for robust pole assignment with repeated poles," *IEEE Trans. Autom. Control*, vol. 61, no. 9, pp. 2370–2385, Sep. 2016.
[45] J. Zhong, *Coupling Design Theory and Method of Complex Electronmechanical System*. Beijing, China: China Machine Press, 2007.

YONG LI received the Ph.D. degree in vehicle engineering from the University of Science and Technology Beijing, Beijing, China, in 2015. He is currently a Lecturer with the Automotive Engineering Research Institute, Jiangsu University, China. His research interests include permanent magnet synchronous motor control and drives, complex electromechanical coupling systems, and parameters matching and optimization of powertrain system in electrified vehicles.

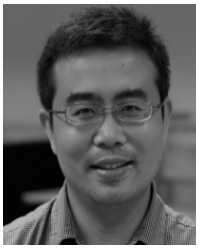

BIN LI received the Ph.D. degree from Shanghai Jiao Tong University, Shanghai, China, in 2010. He was a Research Fellow on next generation electric vehicle project with the University of Waterloo and on mobile robotic control project with McGill University. He is currently a Researcher with Concordia University, Canada, where he focuses on active chassis control systems and active safety control for commercial vehicles and electrified vehicles (EVs). His research interests focus on road vehicle system modeling, dynamics and control, EVs, integrated vehicle motion control, driver behaviour modeling and analysis, and automated vehicle control.

XING XU received the Ph.D. degree in agricultural electrification and automation from Jiangsu University, China, in 2010. He is currently an Associate Professor with the Automotive Engineering Research Institute, Jiangsu University. His research interests include vehicle system dynamics control.

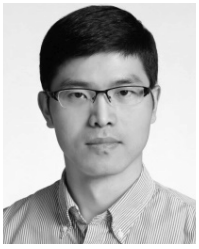

XIAODONG SUN received the B.Sc. degree in electrical engineering and the M.Sc. and Ph.D. degrees in control engineering from Jiangsu University, Zhenjiang, China, in 2004, 2008, and 2011, respectively. From 2014 to 2015, he was a Visiting Scholar with the School of Electrical, Mechanical, and Mechatronic Systems, University of Technology Sydney, Sydney, NSW, Australia. Since 2004, he has been with Jiangsu University, where he is currently a Professor with the Automotive Engineering Research Institute. His research interests include electrical machines and drives, drives and control for electric vehicles, and intelligent control.